



Highly efficient polaritonic light-emitting diodes with angle-independent narrowband emission

Received: 2 July 2022

Accepted: 26 January 2023

Published online: 16 March 2023

Check for updates

Andreas Mischok^{1,2}✉, Sabina Hillebrandt^{1,2}, Seonil Kwon^{1,2} & Malte C. Gather^{1,2}✉

Angle-independent narrowband emission is required for many optoelectronic devices, ranging from high-definition displays to sensors. However, emerging materials for electroluminescent devices, such as organics and perovskites, show spectrally broad emission due to intrinsic disorder. Coupling this emission to an optical resonance reduces the linewidth, but at the cost of inheriting the severe angular dispersion of the resonator. Strongly coupling a dispersionless exciton state to a narrowband optical microcavity could overcome this issue; however, electrically pumped emission from the resulting polaritons is typically hampered by poor efficiencies. Here we present a universal concept for polariton-based emission from organic light-emitting diodes by introducing an assistant strong coupling layer, thereby avoiding quenching-induced efficiency losses. We realize red- and green-emitting, narrowband (full-width at half-maximum of less than 20 nm) and spectrally tunable polaritonic organic light-emitting diodes with up to 10% external quantum efficiency and high luminance ($>20,000 \text{ cd m}^{-2}$ at 5 V). By optimizing cavity detuning and coupling strength, we achieve emission with ultralow dispersion ($<10 \text{ nm}$ spectral shift at 60° tilt). These results may have wide-reaching implications for on-demand polariton emission and demonstrate the practical relevance of strong light–matter coupling for next-generation optoelectronics, particularly display technology.

When a material with a strong excitonic resonance is inserted into a high-quality microcavity (MC), strong coupling and hybridization of light and matter can occur and lead to the formation of exciton-polariton quasiparticles. Polaritons inherit a number of advantageous characteristics from their constituents; for example, they show the high interaction strength of excitons and are readily observable as emitted photons. Thus, polaritons offer a highly attractive platform for various applications, for example, transistors¹, photodiodes^{2–4}, single-photon sources⁵ and detectors⁶, and polariton lasers^{7–11}. However, to realize

this potential, there is need for a readily available polariton-based electroluminescent device that works under ambient conditions, that is, a polariton light-emitting diode (LED). Attempts to use GaAs to realize such LEDs have had limited success as the weak exciton binding in GaAs complicates operation at non-cryogenic temperatures¹².

Organic semiconductors offer large exciton binding energies and high oscillator strengths; thus, polaritons are stable in these materials, even at room temperature¹³. Driving MC-based organic light-emitting diodes (OLEDs) into the strong coupling regime has indeed allowed the

¹Organic Semiconductor Centre, SUPA, School of Physics and Astronomy, University of St Andrews, North Haugh, UK. ²Humboldt Centre for Nano- and Biophotonics, Department of Chemistry, University of Cologne, Köln, Germany. ✉e-mail: andreas.mischok@uni-koeln.de; malte.gather@uni-koeln.de

realization of room-temperature polariton LEDs^{12,14–22}. However, these polaritonic organic light-emitting diodes (POLEDs) have shown very low external quantum efficiency (EQE) and low brightness because strongly absorbing bulk materials had to be used as the emissive layer (EML) to achieve strong coupling. Such EMLs often have low photoluminescence quantum yields compared with doped EMLs used in state-of-the-art OLEDs, all of which operate in the weak coupling regime²³. Coupling inorganic and organic resonators^{24,25} and employing the radiative pumping of polaritons^{26–28} have been proposed to improve the efficiency of OLEDs. Nevertheless, to the best of our knowledge, the highest EQEs reported so far for a single-cavity POLED and coupled weak-strong cavity architecture are only 0.2% (ref. ²²) and 1.2% (ref. ²⁸), respectively. In comparison, weakly coupled MC OLEDs readily achieve EQEs above 20% (refs. ^{29–31}).

In this work, we demonstrate highly efficient, electrically driven polariton generation and light emission from both red- and green-emitting POLEDs. To realize efficient operation, we add an assistant strong coupling layer into the second field maximum of an MC OLED that uses a doped EML with high luminescence quantum yield. The resulting devices retain more than 70% of the EQE achieved by weakly coupled reference OLEDs and, at 5 V forward bias, they reach luminance values of over 20,000 cd m⁻². The characteristics of our devices are dominated by polariton formation, with emission exclusively emanating from the lower polariton branch (LPB). Varying the thicknesses of the cavity and the strong coupling layer enables us to tune the emission characteristics and to enter the ultrastrong coupling (USC) regime without major losses in performance.

In addition to offering a strategy to realize polariton emission, our POLEDs enable the development of OLED displays with viewing-angle-independent emission colour and improved colour saturation. Many organic materials and the resulting OLEDs show broad emission spectra due to the intrinsic disorder in these materials. Using a weakly coupled MC yields more narrowband emission and can improve the colour saturation, but generally results in strong angular dispersion^{29,32,33} and a clearly visible change in the emission colour with increasing viewing angle, which is problematic for OLED displays³⁴ and emerging applications in biosensing and imaging³⁵. Angular dispersion in MC OLEDs can be managed by the use of external²⁹ or internal^{36,37} scattering elements or other designs^{38,39} that mix the different angular components; however, these approaches substantially increase the spectral bandwidth and thus reduce the colour purity. In contrast, we show here that the hybridized light-matter polaritons in our POLEDs can be tuned to exhibit flat, exciton-like angular dispersion, which eliminates any noticeable colour change with angle and maintains the high colour purity and efficiency of an MC OLED. Thus, beyond their use in polaritonics, our POLEDs offer desirable properties for displays and other emerging applications requiring narrowband and angle-independent light sources.

Results and discussion

Realization of POLEDs

We based the development of our POLED on an efficient phosphorescent MC OLED^{31,40} that operates in the weak coupling regime and that serves as a reference design. This reference OLED consists of a thin Ag bottom contact (25 nm) and a thick Ag top contact that form a second-order bottom-emitting MC and sandwich a thick p-doped hole transport layer (HTL), electron blocking layer (EBL), EML, hole blocking layer (HBL) and n-doped electron transport layer (ETL) (Fig. 1a and Supplementary Fig. 1). Transfer matrix simulations were performed to optimize light outcoupling at the emission wavelength of the Ir(MDQ)₂(acac)-based EML. The reference OLED generates a narrowband emission spectrum that can be tuned in wavelength by adjusting the thickness of the charge transport layers. The use of doped charge transport layers means that this tuning has a negligible impact on the operating voltage of the final device as well as ensures low-voltage operation.

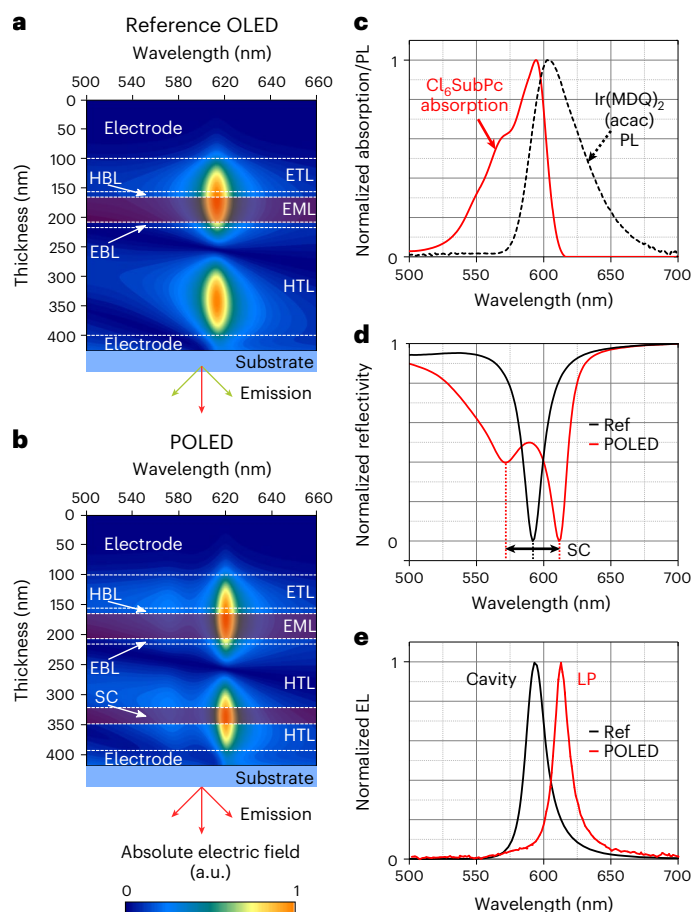


Fig. 1 | Concept and initial demonstration of the POLED based on an assistant strong coupling layer. **a**, Structure and electric-field distribution of the reference OLED comprising two reflective Ag electrodes forming an MC, spiro-TTB:F₆T CNNQ at 4 wt% as the p-doped HTL, NPB as the EBL, NPB doped with Ir(MDQ)₂(acac) at 10 wt% as the EML, BAQ as the HBL and BPheN:Cs at 3 wt% as the n-doped ETL. **b**, Structure and electric-field distribution of the POLED with a 24-nm-thick assistant strong coupling (SC) layer of the Cl₆SubPc absorber (blended at 1:1 with spiro-TTB) inserted into the HTL at the location of peak optical field strength. **c**, Absorption spectrum of Cl₆SubPc (red solid line) and photoluminescence (PL) spectrum of Ir(MDQ)₂(acac) (black dashed line). **d**, Reflectivity spectra at 20° angle of incidence for a reference MC OLED without the strong coupling layer (black) and POLED (red). The strong coupling of cavity photons and Cl₆SubPc excitons leads to splitting of the resonance peak in the POLED reflectivity spectrum, as indicated by the double arrow. **e**, Corresponding EL spectra of both devices at a viewing angle of 20°.

Strong light-matter coupling occurs when the interaction between photons and excitons in the system becomes stronger than the loss rate of either particle. Due to the weakly allowed triplet-to-singlet transition of state-of-the-art phosphorescent emitters like Ir(MDQ)₂(acac) and because their concentration in the EML is relatively low (10 wt% for our devices), these emitters on their own do not exhibit sufficient interaction with cavity photons for strong coupling to occur. Instead, we hypothesize that the addition of an absorber with an absorption spectrum complimentary to the emission of Ir(MDQ)₂(acac) in the second field maximum of the cavity can facilitate strong coupling without jeopardizing the OLED performance. This strategy splits up the processes of electroluminescence (EL) and polariton formation and thus efficiently realizes both processes.

Cl₆SubPc, commonly used in non-fullerene organic solar cells, has recently been shown to induce strong coupling, even in very thin films, due to its strong absorption and low Stokes shift³.

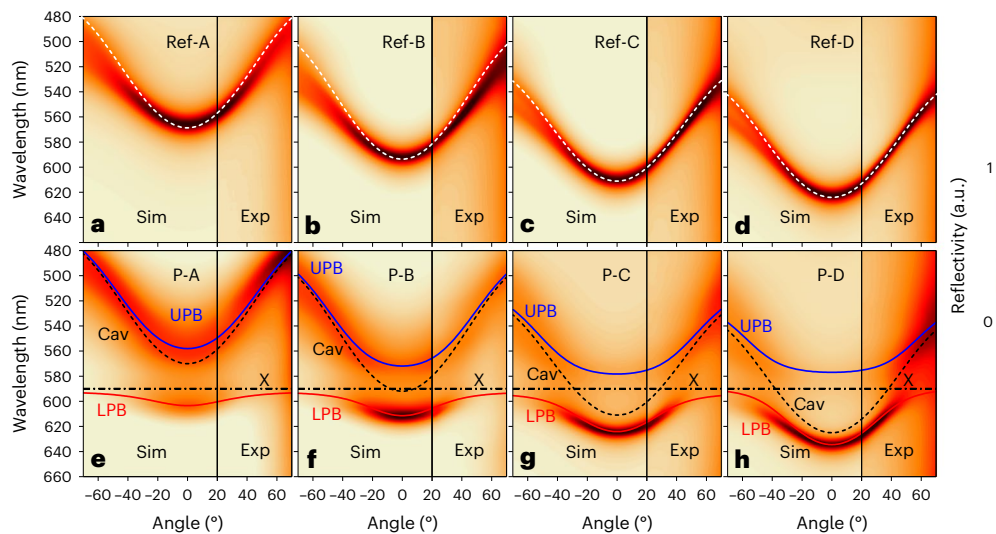


Fig. 2 | Polariton formation and tuning. **a–h**, Simulated (Sim; left) and measured (Exp; right) reflectivity spectra of weakly coupled reference OLEDs (**a–d**) and POLEDs with a strong coupling layer (**e–h**) on a false-colour scale. The cavity thickness increases from left to right; the reference OLEDs and POLEDs in the same column have the same total optical thickness. The white and black lines

indicate the calculated position of the cavity mode (dashed lines) and exciton (X; dash-dotted lines) in the reference OLEDs and POLEDs, respectively. The solid blue and red lines in **e–h** show the position of the UPB and LPB, respectively, as obtained from the CO model. See Supplementary Tables 1 and 2 for layer thicknesses of each device.

The absorption of Cl_6SubPc is nearly perfectly complementary to the emission of $\text{Ir}(\text{MDQ})_2(\text{acac})$ (Fig. 1c). As the position of the highest occupied molecular orbital of Cl_6SubPc at -5.6 eV (ref. ⁴¹) is close to that of the Spiro-TTB-based HTL at -5.3 eV, we expect that a thin layer of Cl_6SubPc can be inserted into the HTL without creating a substantial energy barrier to hole transport. To further reduce the impact of adding Cl_6SubPc on electrical performance and avoid crystallization ⁴², we co-evaporated Cl_6SubPc with Spiro-TTB at a volumetric ratio of 1:1.

To realize our POLED, a 24-nm-thick layer of the Spiro-TTB: Cl_6SubPc blend was positioned within the HTL of the OLED, so that the layer was exactly located in the field maximum of the cavity mode at the wavelength of the Cl_6SubPc exciton (590 nm; Fig. 1b). Simultaneously, the thickness of the HTL was reduced by 32 nm to maintain the same overall optical thickness as the reference MC OLEDs (Supplementary Tables 1 and 2).

Although the reflectivity spectrum of the reference OLED has a single characteristic dip associated with the cavity mode, the reflectivity spectrum of the POLED shows a distinct splitting into an upper and lower polariton (Fig. 1d), which is evidence of strong coupling between the cavity photons and material excitons. The presence of strong coupling was further confirmed by a redshift in the EL, which was aligned with the cavity mode for the reference OLED but exclusively emanated from the LPB in the POLED (Fig. 1e and Supplementary Fig. 2). Despite the different nature of their emission processes, both reference OLED and POLED have narrowband emission spectra, with Lorentzian linewidths of 16 nm—much sharper than the emission spectrum of a conventional, non-cavity-based $\text{Ir}(\text{MDQ})_2(\text{acac})$ OLED (70 nm linewidth; Supplementary Fig. 7). To assess the contributions of $\text{Ir}(\text{MDQ})_2(\text{acac})$ and Cl_6SubPc to strong coupling, we have performed a careful analysis of the absorption spectrum of the individual layers combined with transfer matrix simulations of the intracavity absorption (Supplementary Fig. 3 and Supplementary Note 1).

Variation in cavity detuning

Next, we explored how varying the optical thickness and thus detuning the cavity mode relative to the exciton energy affects polariton formation and angular dispersion. Figure 2 summarizes the modelled and experimentally measured angle-resolved reflectivity spectra of weakly coupled reference OLEDs (Ref-A to Ref-D) with a range of cavity

thicknesses as well as the corresponding strongly coupled POLEDs (P-A to P-D). The spectra of the POLEDs show clear anti-crossing of the upper polariton branches (UPBs) and LPBs, confirming the presence of strong coupling in the POLEDs over the entire range of detuning investigated.

To measure the coupling strength in the POLEDs, we compared our observations with the predictions of the coupled oscillator (CO) Hamiltonian as⁴³

$$\begin{pmatrix} E_{\text{Cav}}(\theta) & G \\ G & E_X \end{pmatrix} \begin{pmatrix} F_{\text{Cav}} \\ F_X \end{pmatrix} = E_{\text{Pol}}(\theta) \begin{pmatrix} F_{\text{Cav}} \\ F_X \end{pmatrix}$$

where $E_{\text{Cav}}(\theta)$ and E_X are the cavity and exciton energies, respectively; G is the Rabi splitting of the lower and upper polariton; F_{Cav} and F_X are the cavity photon fraction and exciton fraction of the polariton, respectively; $E_{\text{Pol}}(\theta)$ is the polariton energy; and θ is the outcoupling angle. The energy of the cavity mode $E_{\text{Cav}}(\theta)$ was extracted from the reflectivity of the reference OLEDs and the exciton energy was determined from the Cl_6SubPc absorption spectrum. By fitting the Rabi splitting for all the POLEDs, we obtained excellent agreement with the reflectivity spectra for $G = 140$ meV (Fig. 2, solid lines). The analysis with the CO Hamiltonian also shows that the exciton fraction in the LPB is the highest for the POLEDs with the highest E_{Cav} and is larger for larger angles (Supplementary Fig. 4). Consequently, we observe a predominantly flat, exciton-like dispersion of the LPB in devices P-A and P-B. As a rule, high coupling strengths and blue-detuned MC appear to lead to particularly flat angular dispersion of the LPB.

Electrical performance

Figure 3 shows the current–voltage–luminance and the EQE versus luminance characteristics for the reference OLEDs (Ref-A to Ref-D) and POLEDs (P-A to P-D). Comparing the OLEDs, the most important observations are as follows. (1) Both sets of devices reach high luminance values above $20,000 \text{ cd m}^{-2}$ at a low operating voltage of 5 V. (2) The introduction of the absorbing strong coupling layer does not lead to a notable change in turn-on voltage but causes a reduction in current density (by approximately 10–50% depending on the device and applied voltage). (3) The EQE increases from Ref-A to Ref-D and from P-A to P-D due to an increase in outcoupling efficiency for more

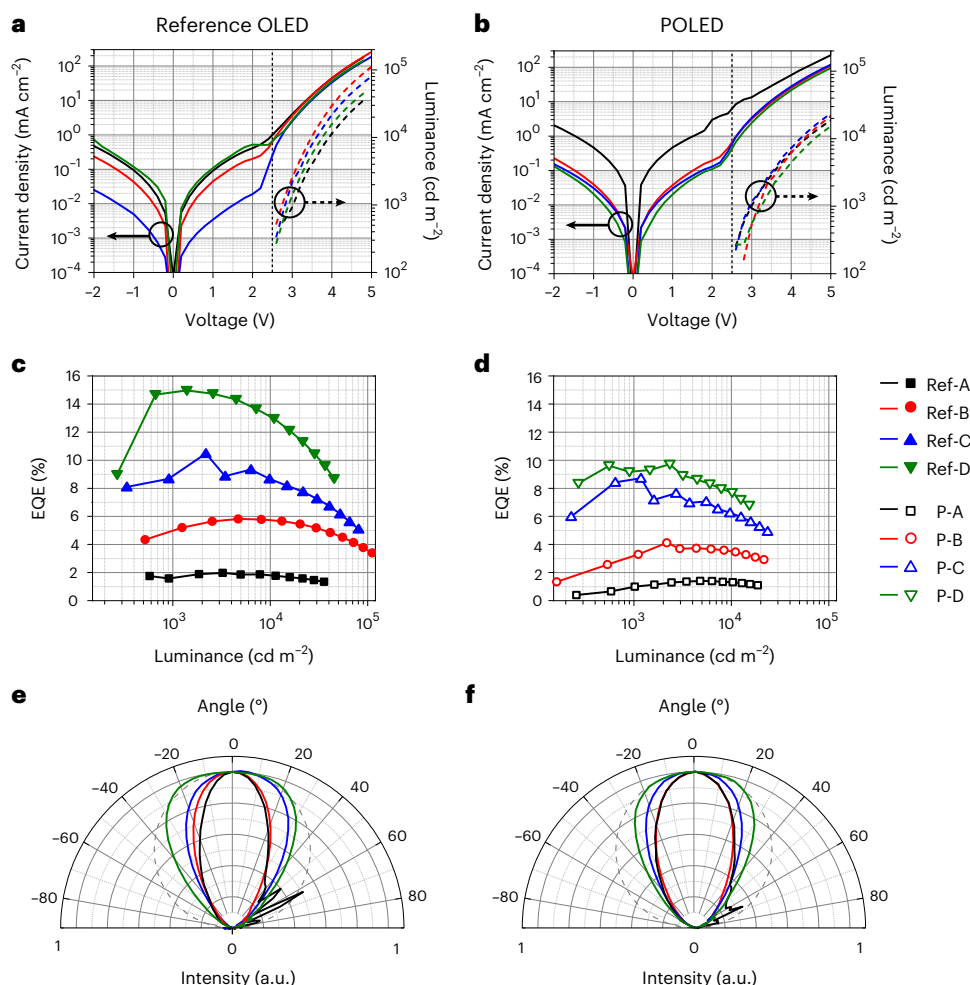


Fig. 3 | Device performance. **a,b**, Current density and luminance versus voltage for the reference OLEDs (**a**) and POLEDs (**b**). All the devices turn-on at around 2.5 V (dashed vertical line) and reach a luminance of over 10,000 cd m⁻² at 5.0 V, irrespective of whether the strong coupling layer is present in the device or not. **c,d**, EQE versus luminance for the reference OLEDs (**c**) and POLEDs (**d**). **e,f**, Angle-

resolved emission intensity of the reference OLEDs (**e**) and POLEDs (**f**), showing directional emission for all devices. The dashed lines indicate the profile of a Lambertian emitter. The EQE values in **c** and **d** take the actual, non-Lambertian angular emission characteristics of each device into account.

red-tuned devices. (4) The POLEDs reach approximately 70% of the EQE of the corresponding reference OLEDs, peaking at an EQE of 9.7% for P-D. (5) The roll-off in efficiency⁴⁴ at high luminance is not much affected by the strong coupling layer (for example, critical current density $J_{90\%} = 21 \text{ mA cm}^{-2}$ for P-D versus 15 mA cm^{-2} for Ref-D), indicating that the polariton conversion process in the devices operates far from saturation. (6) The POLEDs retain the strong directional emission of the MC devices (Fig. 3e,f).

Angular colour stability and flexible POLEDs

The transformation of cavity photons into polaritons strongly alters the angular dispersion of light emitted by our devices. In particular, as the dispersion of the LPB becomes more exciton-like, its wavelength shift with angle is greatly reduced. As emission exclusively occurs from the LPB in our POLEDs, this leads to greatly improved angular colour stability. Figure 4a,b compares the angle-resolved EL of the weakly coupled MC OLED (Ref-C) to P-A and P-B, all of which emit at around 610 nm at 0° observation angle (Supplementary Figs. 5 and 6 show the angle-resolved spectra of all the devices in this study). Although the colour of the reference OLED visually changes from red to yellow on tilting, no colour change is noticeable for the POLEDs. The peak emission of the reference OLED blueshifts

by 45 nm between 0° and 60°. In contrast, the POLEDs only show a wavelength shift of 8 nm (P-A) and 15 nm (P-B) over this range. The residual wavelength shifts of the POLEDs over the 0°–60° cone are, thus, smaller than or comparable with the full-width at half-maximum of their respective emission spectra (P-A, 18 nm full-width at half-maximum; P-B, 12 nm).

Next, we developed a substrateless and flexible POLED in which a thin-film encapsulation stack—based on layers of parylene C and Al₂O₃/ZrO₂ nanolaminates—acts as both moisture and oxygen barrier and a quasi-substrate⁴⁵, thus reducing the total thickness of the device to below 30 μm (Fig. 4c). The resulting flexible POLED exhibits narrowband (full-width at half-maximum, 25 nm) and virtually angle-independent emission spectra (13 nm shift from 0° to 60° viewing angle), whereas a flexible reference MC OLED shows the expected large angular dispersion (Fig. 4d). Due to the interaction between the OLED MC and thin-film encapsulation stack, the emission spectrum of the flexible POLED is slightly broader than the spectra of our devices on rigid substrates. In addition, weak parabolic cavity modes originating from the parylene C layers are visible in the spectrum; however, this does not diminish the visually perceived colour stability of the device. Even under extreme bending (radius of curvature, <5 mm), no variation in emission colour is visible (Fig. 4e).

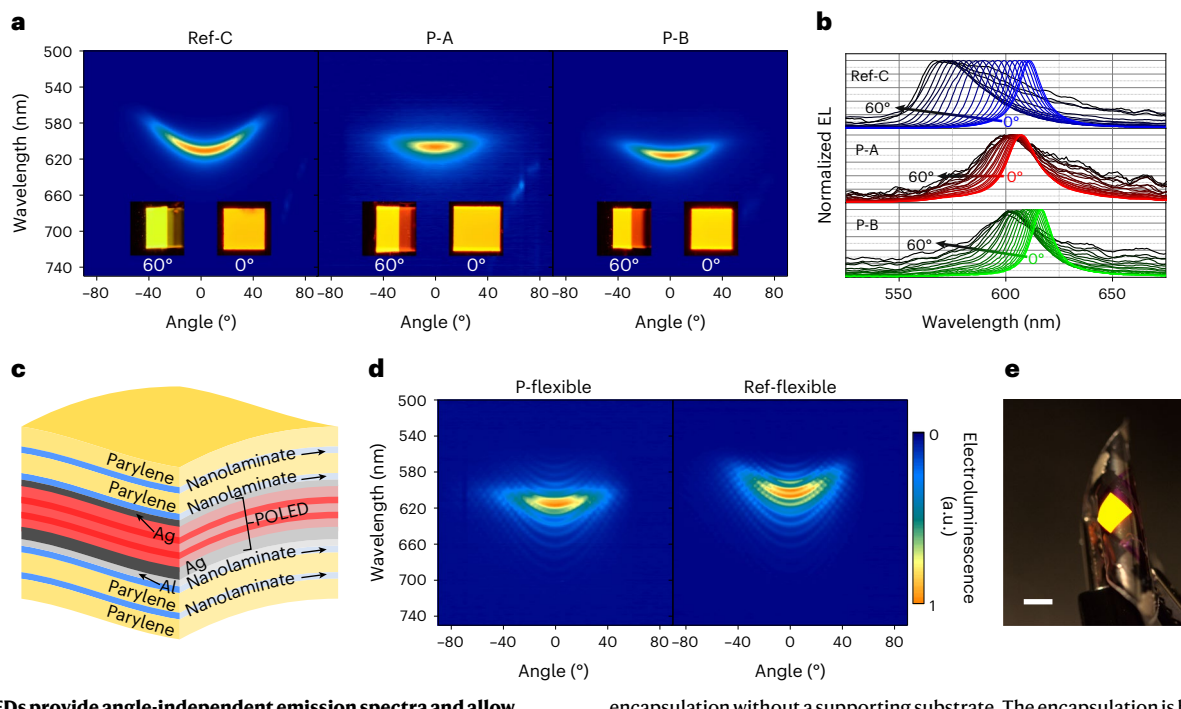


Fig. 4 | POLEDs provide angle-independent emission spectra and allow mechanically flexible devices. **a**, Angle-resolved EL spectra of Ref-C, P-A and P-B on a false-colour scale. The insets show the photographs of the emission of each OLED at observation angles of 0° and 60°. The pixel size is $2 \times 2 \text{ mm}^2$. **b**, Normalized EL spectra of the devices in **a** for angles between 0° and 60°. All the spectra were recorded at a constant current density of 25 mA cm^{-2} . **c**, Device structure of the flexible POLED sandwiched by flexible thin-film

encapsulation without a supporting substrate. The encapsulation is based on layers of parylene C and a metal oxide nanolaminates. **d**, Angle-resolved EL spectrum for a flexible POLED (P-flexible) and flexible reference OLED (Ref-flexible; also uses an MC, but without a strong coupling layer). **e**, Photograph of the emission from a rolled-up, flexible POLED showing no change in emission colour, irrespective of the viewing and bending angles. Scale bar, 4 mm.

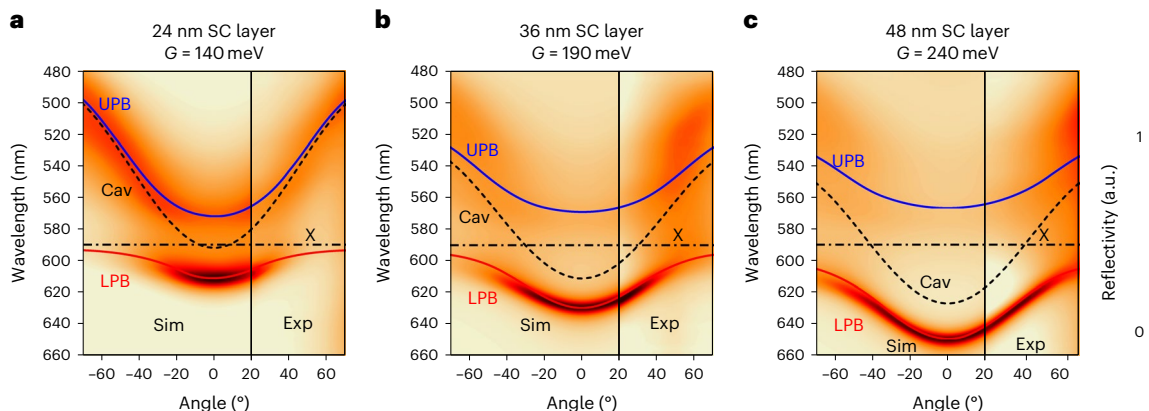


Fig. 5 | Variation in coupling strength in red POLEDs. **a–c**, Simulated (Sim; left) and measured (Exp; right) reflectivity spectra for POLEDs with strong coupling layers of different thicknesses, resulting in increasing Rabi splitting: 24 nm thickness, $G = 140 \text{ meV}$ (**a**); 36 nm thickness, $G = 190 \text{ meV}$ (**b**); 48 nm thickness,

$G = 240 \text{ meV}$ (**c**). The black lines indicate the calculated position of the cavity modes (dashed lines) and exciton line (X; dash-dotted lines). The solid blue and red lines show the position of the UPB and LPB, respectively, as obtained from the CO model. See Supplementary Table 2 for layer thicknesses of each device.

Tuning of coupling strength

As we introduce strong coupling in our POLEDs in a manner that separates polariton formation from OLED emission, the coupling strength can be tuned without substantially changing the electrical properties of the devices. Figure 5a–c shows the polariton dispersion for a series of devices with strong coupling layers of increasing thickness. Here the Rabi splitting, as determined by CO modelling, increases from 140 meV (for a 24 nm spiro-TTB:Cl₆SubPc layer) to 190 meV (for 36 nm) and 240 meV (for 48 nm), demonstrating a direct tuning of coupling strength (Supplementary Fig. 8 shows the device performance). As the

emission still occurs exclusively from the LPB (Supplementary Fig. 9), we conclude that the OLED characteristics are dominated by polariton formation, and thus, they can be adjusted over a wide range by simply changing the thickness of the strong coupling layer.

Fully optimized POLEDs with green emission

Our approach is not limited to the specific combination of emitter and strong coupling materials presented above. To show the universality of the concept, we realized POLEDs comprising the phosphorescent green emitter Ir(ppy)₃(acac) combined with an assistant strong coupling

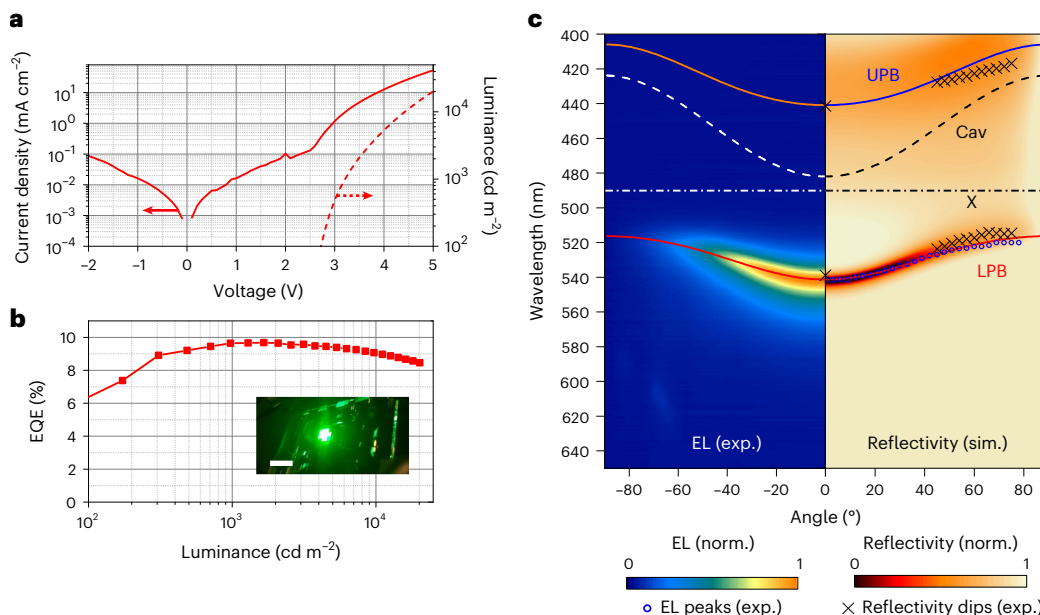


Fig. 6 | Optimized green POLED in the USC regime. **a**, Current density–voltage–luminance characteristics, showing that the device reaches a luminance of $20,000 \text{ cd m}^{-2}$ at 5 V in the presence of a thick assistant strong coupling layer. **b**, EQE of the device, reaching a peak of 9.7% at $\sim 1,500 \text{ cd m}^{-2}$. The inset shows a photograph of POLED emission. Scale bar, 5 mm. **c**, Angle-resolved, measured

EL intensity (exp.; left) and simulated device reflectivity (sim.; right) of the USC POLED. The crosses show the positions of the minima in the measured reflectivity spectra and the circles show the peak position of the measured EL intensity. The lines denote the calculated polariton branches (solid), cavity mode (dashed) and exciton energy (dash-dotted).

layer of the coumarin dye C545T (refs. ^{22,43}). As in our original material system, this material pair exhibits complimentary absorption (C545T) and emission ($\text{Ir}(\text{ppy})_2(\text{acac})$) spectra.

Adapting an MC OLED reported previously⁴⁶, we fabricated a set of reference OLEDs and POLEDs with these materials (Supplementary Figs. 10 and 11 and Supplementary Tables 4 and 5). We then analysed the angle-resolved reflectivity, angle-resolved EL and electrical performance, as described above for the red-emitting devices. Again, we observed angle-independent polariton emission with high luminance (here, $>100,000 \text{ cd m}^{-2}$ at 5 V) and peak EQE of 10.2% (Supplementary Figs. 12 and 13). As before, the efficiency of the green POLEDs is broadly comparable with the efficiency of the corresponding reference OLEDs. However, the green-emitting POLEDs reach lower current densities than the reference OLEDs, suggesting that the low hole mobility of the C545T layer introduces a charge imbalance. This illustrates the importance of choosing either an assistant strong coupling material with adequate charge mobility or using the blended layer approach that we applied for red-emitting POLEDs.

Like for the red-emitting POLEDs, the coupling strength of the green system can be tuned by varying the thickness of the strong coupling layer (Supplementary Fig. 14); in fact, the combination of $\text{Ir}(\text{ppy})_2(\text{acac})$ and C545T facilitates even higher coupling strengths. Combining optical tuning via the cavity thickness with tuning of the coupling strength, we realized a fully optimized device that operates in the USC regime and for which the polariton shows a high exciton fraction. Figure 6 summarizes the characteristics of this green USC POLED with an optimized stack (Supplementary Table 6) that includes a 60-nm-thick layer of C545T, pushing the Rabi splitting to 520 meV (that is, a coupling strength of 10.3% of the bare exciton energy), and creating highly favourable outcoupling conditions for light emission. This optimized device achieved an EQE of 9.7%, a luminance above $20,000 \text{ cd m}^{-2}$ at 5 V and a flat dispersion with a shift of $<20 \text{ nm}$ between 0 and 60° . USC POLEDs with different detunings, along with a detailed analysis of the optimized device, are shown in Supplementary Figs. 15–17 and Supplementary Note 2.

Discussion

By adding a strong coupling layer in the second field maximum of a second-order cavity device, a state-of-the-art phosphorescent OLED structure was transformed into a bright and highly efficient source of on-demand, electrically pumped polariton emission. Combining efficient Ir-based emitters with either Cl_6SubPc in the red or C545T in the green yielded highly tunable polariton emission, with EQEs of 10% and luminance levels over $20,000 \text{ cd m}^{-2}$ at 5 V forward bias. The assistant strong coupling layer ensures that the overall device characteristics remain dominated by the strongly coupled cavity; at a sufficiently large coupling strength, even the USC regime is reached without introducing major losses in device efficiency. Compared with previously demonstrated POLEDs^{22,28}, this represents an increase in EQE of at least an order of magnitude and an increase in luminance and luminous efficacy of at least two orders of magnitude, thus demonstrating that such devices can reach application-relevant performance. Combining our concept with thin-film encapsulation, we also realized—to the best of our knowledge—the first demonstration of a mechanically flexible polariton LED.

Earlier POLEDs were typically based on bulk emitter layers that generally show low luminescence quantum yields and do not support triplet harvesting mechanisms. By decoupling light emission and polariton formation, we avoid the catastrophic losses in device efficiency that have plagued POLEDs so far and gain access to phosphorescent emitters for our design. The realization of efficient red and green POLEDs indicates that the majority of currently used emitter materials can be employed in our polariton devices, as long as they are combined with the appropriate assistant strong coupling layer. Given the enormous breadth of OLED structures known today, this strategy, therefore, unlocks the entire visible spectrum and parts of the near-infrared spectrum for efficient polariton emission. In addition, this universality provides numerous possibilities to reduce the remaining gap in EQE between POLEDs and conventional OLEDs, for example, through the application of the latest-generation phosphorescent and thermally activated delayed fluorescence emitters including

emitter systems showing strongly horizontal dipole orientation^{47,48}, as well as the integration of capping layers and other light extraction modalities⁴⁹.

In the future, the POLEDs developed here could be adopted to use a short-excited-state-lifetime fluorescent emitter and a high-luminescence-quantum-yield strong coupling layer. Such an architecture would provide a promising monolithic pathway to electrically pumped polariton lasing in organic systems, for example, by combining metallic contacts with high-optical-quality distributed Bragg reflectors^{50,51}.

Beyond their relevance to lasers and fundamental studies of polariton phenomena, a number of features render the POLEDs developed in this work particularly attractive for display applications: most importantly, by appropriately tuning the emissive lower polariton state, the angular dependence of the emission wavelength in these narrowband devices can be greatly reduced. This enables the emission of more saturated colours than possible with current OLED technology, without introducing a change in the perceived colour when looking at the device from different angles. In the past, MC dispersion has prevented or complicated the use of MC OLEDs based on metallic thin-film electrodes and often necessitated the application of transparent conductive oxides for one of the electrodes. However, the brittle nature of many conductive oxides and the scarcity of indium, which is a common component in these devices⁵², makes a move to OLEDs based entirely on thin metal electrodes highly desirable—from a cost perspective as well as to improve the robustness and reliability of future flexible displays. Furthermore, the integration of OLEDs on driver backplanes, particularly those based on silicon complementary metal–oxide–semiconductor chips, requires the use of top-emitting OLED architectures. For these, metal–metal MC OLEDs are again preferred as the deposition of transparent conductive oxides on the OLED stack can damage the organic material. Last, the rearrangement of exciton energies to polariton states that occurs in a POLED can reduce the effective optical bandgap of the system and enable tuning of the singlet energies, and this strategy may allow to enhance device efficiency through the improved recycling of triplet states^{3,53–56}.

Online content

Any methods, additional references, Nature Portfolio reporting summaries, source data, extended data, supplementary information, acknowledgements, peer review information; details of author contributions and competing interests; and statements of data and code availability are available at <https://doi.org/10.1038/s41566-023-01164-6>.

References

- Zasedatelev, A. V. et al. A room-temperature organic polariton transistor. *Nat. Photon.* **13**, 378–383 (2019).
- Eizner, E., Brodeur, J., Barachati, F., Sridharan, A. & Kéna-Cohen, S. Organic photodiodes with an extended responsivity using ultrastrong light-matter coupling. *ACS Photonics* **5**, 2921–2927 (2018).
- Nikolis, V. C. et al. Strong light-matter coupling for reduced photon energy losses in organic photovoltaics. *Nat. Commun.* **10**, 3706 (2019).
- Mischok, A. et al. Spectroscopic near-infrared photodetectors enabled by strong light-matter coupling in (6,5) single-walled carbon nanotubes. *J. Chem. Phys.* **153**, 201104 (2020).
- Muñoz-Matutano, G. et al. Emergence of quantum correlations from interacting fibre-cavity polaritons. *Nat. Mater.* **18**, 213–218 (2019).
- Zasedatelev, A. V. et al. Single-photon nonlinearity at room temperature. *Nature* **597**, 493–497 (2021).
- Daskalakis, K. S., Maier, S. A., Murray, R. & Kéna-Cohen, S. Nonlinear interactions in an organic polariton condensate. *Nat. Mater.* **13**, 271–278 (2014).
- Plumhof, J. D., Stöferle, T., Mai, L., Scherf, U. & Mahrt, R. F. Room-temperature Bose–Einstein condensation of cavity exciton-polaritons in a polymer. *Nat. Mater.* **13**, 247–252 (2014).
- Rajendran, S. K. et al. Low threshold polariton lasing from a solution-processed organic semiconductor in a planar microcavity. *Adv. Opt. Mater.* **7**, 1801791 (2019).
- Anni, M. & Lattante, S. *Organic Lasers: Fundamentals, Developments, and Applications*. Vol. 1 (CRC Press, 2018).
- Le Roux, F., Mischok, A., Bradley, D. D. C. & Gather, M. C. Efficient anisotropic polariton lasing using molecular conformation and orientation in organic microcavities. *Adv. Funct. Mater.* **32**, 2209241 (2022).
- Tsintzos, S. I., Pelekanos, N. T., Konstantinidis, G., Hatzopoulos, Z. & Savvidis, P. G. A GaAs polariton light-emitting diode operating near room temperature. *Nature* **453**, 372–375 (2008).
- Lidzey, D. G. et al. Room temperature polariton emission from strongly coupled organic semiconductor microcavities. *Phys. Rev. Lett.* **82**, 3316–3319 (1999).
- Christogiannis, N. et al. Characterizing the electroluminescence emission from a strongly coupled organic semiconductor microcavity LED. *Adv. Opt. Mater.* **1**, 503–509 (2013).
- Gambino, S. et al. Ultrastrong light-matter coupling in electroluminescent organic microcavities. *Appl. Mater. Today* **1**, 33–36 (2015).
- Mazzeo, M. et al. Ultrastrong light-matter coupling in electrically doped microcavity organic light emitting diodes. *Appl. Phys. Lett.* **104**, 233303 (2014).
- Gambino, S. et al. Exploring light-matter interaction phenomena under ultrastrong coupling regime. *ACS Photonics* **1**, 1042–1048 (2014).
- Dokiya, S. et al. Strong exciton-photon coupling in organic microcavity electroluminescence devices with thiophene/phenylene co-oligomer derivatives. *Appl. Phys. Express* **12**, 111002 (2019).
- Tischler, J. R. et al. Solid state cavity QED: strong coupling in organic thin films. *Org. Electron.* **8**, 94–113 (2007).
- Gubbin, C. R., Maier, S. A. & Kéna-Cohen, S. Low-voltage polariton electroluminescence from an ultrastrongly coupled organic light-emitting diode. *Appl. Phys. Lett.* **104**, 233302 (2014).
- Chang, J.-F. et al. Highly efficient polariton emission of an ultrastrongly coupled MDMO-PPV OLED. *Jpn. J. Appl. Phys.* **61**, 020906 (2022).
- Genco, A. et al. Bright polariton coumarin-based OLEDs operating in the ultrastrong coupling regime. *Adv. Opt. Mater.* **6**, 1800364 (2018).
- Wei, Q. et al. Small-molecule emitters with high quantum efficiency: mechanisms, structures, and applications in OLED devices. *Adv. Opt. Mater.* **6**, 1800512 (2018).
- Jayaprakash, R. et al. A hybrid organic–inorganic polariton LED. *Light Sci. Appl.* **8**, 81 (2019).
- Paschos, G. G. et al. Hybrid organic–inorganic polariton laser. *Sci. Rep.* **7**, 11377 (2017).
- Lodden, G. H. & Holmes, R. J. Polarization splitting in polariton electroluminescence from an organic semiconductor microcavity with metallic reflectors. *Appl. Phys. Lett.* **98**, 233301 (2011).
- Grant, R. T. et al. Efficient radiative pumping of polaritons in a strongly coupled microcavity by a fluorescent molecular dye. *Adv. Opt. Mater.* **4**, 1615–1623 (2016).
- Chang, J.-F. et al. Development of a highly efficient, strongly coupled organic light-emitting diode based on intracavity pumping architecture. *Opt. Express* **28**, 39781–39789 (2020).
- Meerheim, R., Nitsche, R. & Leo, K. High-efficiency monochrome organic light emitting diodes employing enhanced microcavities. *Appl. Phys. Lett.* **93**, 043310 (2008).

30. Xiang, C., Koo, W., So, F., Sasabe, H. & Kido, J. A systematic study on efficiency enhancements in phosphorescent green, red and blue microcavity organic light emitting devices. *Light Sci. Appl.* **2**, e74 (2013).
31. Hillebrandt, S. et al. High brightness, highly directional organic light-emitting diodes as light sources for future light-amplifying prosthetics in the optogenetic management of vision loss. *Adv. Opt. Mater.* **2200877** (2022).
32. Genco, A. et al. High quality factor microcavity OLED employing metal-free electrically active Bragg mirrors. *Org. Electron.* **62**, 174–180 (2018).
33. Zang, C. et al. Top-emitting thermally activated delayed fluorescence organic light-emitting devices with weak light-matter coupling. *Light Sci. Appl.* **10**, 116 (2021).
34. Isphording, A. & Pralle, M. Quantifying angular color stability of organic light-emitting diodes. *Org. Electron.* **11**, 1916–1919 (2010).
35. Murawski, C. et al. Narrowband organic light-emitting diodes for fluorescence microscopy and calcium imaging. *Adv. Mater.* **31**, 1903599 (2019).
36. Gaynor, W. et al. Color in the corners: ITO-free white OLEDs with angular color stability. *Adv. Mater.* **25**, 4006–4013 (2013).
37. Park, C. H. et al. Enhanced light extraction efficiency and viewing angle characteristics of microcavity OLEDs by using a diffusion layer. *Sci. Rep.* **11**, 3430 (2021).
38. Dong, C. et al. Eliminate angular color shift in top emitting OLEDs through cavity design. *J. Soc. Inf. Display* **27**, 469–479 (2019).
39. Tessler, N., Burns, S., Becker, H. & Friend, R. H. Suppressed angular color dispersion in planar microcavities. *Appl. Phys. Lett.* **70**, 556–558 (1997).
40. Murawski, C., Liehm, P., Leo, K. & Gather, M. C. Influence of cavity thickness and emitter orientation on the efficiency roll-off of phosphorescent organic light-emitting diodes. *Adv. Funct. Mater.* **24**, 1117–1124 (2014).
41. Lee, H. et al. Interfacial electronic structure of Cl₆SubPc non-fullerene acceptors in organic photovoltaics using soft X-ray spectroscopies. *Phys. Chem. Chem. Phys.* **19**, 31628–31633 (2017).
42. Kim, J. & Yim, S. Influence of surface morphology evolution of SubPc layers on the performance of SubPc/C₆₀ organic photovoltaic cells. *Appl. Phys. Lett.* **99**, 193303 (2011).
43. Tropf, L. & Gather, M. C. Investigating the onset of the strong coupling regime by fine-tuning the Rabi splitting in multilayer organic microcavities. *Adv. Opt. Mater.* **6**, 1800203 (2018).
44. Murawski, C., Leo, K. & Gather, M. C. Efficiency roll-off in organic light-emitting diodes. *Adv. Mater.* **25**, 6801–6827 (2013).
45. Keum, C. et al. A substrateless, flexible, and water-resistant organic light-emitting diode. *Nat. Commun.* **11**, 6250 (2020).
46. Lian, C., Yoshida, K., Nogues, C. & Samuel, I. D. W. Organic light-emitting diode based fluorescence sensing system for DNA detection. *Adv. Mater. Technol.* **7**, 2100806 (2022).
47. Tenopala-Carmona, F. et al. Identification of the key parameters for horizontal transition dipole orientation in fluorescent and TADF organic light-emitting diodes. *Adv. Mater.* **33**, 2100677 (2021).
48. Chan, C.-Y. et al. Stable pure-blue hyperfluorescence organic light-emitting diodes with high-efficiency and narrow emission. *Nat. Photon.* **15**, 203–207 (2021).
49. Salehi, A., Fu, X., Shin, D. & So, F. Recent advances in OLED optical design. *Adv. Funct. Mater.* **29**, 1808803 (2019).
50. Brückner, R., Lyssenko, V. G., Hofmann, S. & Leo, K. Lasing of Tamm states in highly efficient organic devices based on small-molecule organic semiconductors. *Faraday Discuss.* **174**, 183–201 (2014).
51. Mischok, A. et al. Phase-locked lasing in 1D and 2D patterned metal-organic microcavities. *Laser Photon. Rev.* **12**, 1800054 (2018).
52. Service, R. F. Mission: irreplaceable? *Science* **327**, 1597 (2010).
53. Stranius, K., Hertzog, M. & Börjesson, K. Selective manipulation of electronically excited states through strong light-matter interactions. *Nat. Commun.* **9**, 2273 (2018).
54. Polak, D. et al. Manipulating molecules with strong coupling: harvesting triplet excitons in organic exciton microcavities. *Chem. Sci.* **11**, 343–354 (2020).
55. Eizner, E., Martínez-Martínez, L. A., Yuen-Zhou, J. & Kéna-Cohen, S. Inverting singlet and triplet excited states using strong light-matter coupling. *Sci. Adv.* **5**, eaax4482 (2019).
56. Yu, Y., Mallick, S., Wang, M. & Börjesson, K. Barrier-free reverse-intersystem crossing in organic molecules by strong light-matter coupling. *Nat. Commun.* **12**, 3255 (2021).

Publisher's note Springer Nature remains neutral with regard to jurisdictional claims in published maps and institutional affiliations.

Open Access This article is licensed under a Creative Commons Attribution 4.0 International License, which permits use, sharing, adaptation, distribution and reproduction in any medium or format, as long as you give appropriate credit to the original author(s) and the source, provide a link to the Creative Commons license, and indicate if changes were made. The images or other third party material in this article are included in the article's Creative Commons license, unless indicated otherwise in a credit line to the material. If material is not included in the article's Creative Commons license and your intended use is not permitted by statutory regulation or exceeds the permitted use, you will need to obtain permission directly from the copyright holder. To view a copy of this license, visit <http://creativecommons.org/licenses/by/4.0/>.

© The Author(s) 2023

Methods

OLED materials and fabrication

OLEDs were fabricated via the thermal evaporation of organic and metal thin films at a base pressure of 1×10^{-7} mbar (Angstrom EvoVac) onto 1.1-mm-thick glass substrates. The materials used were as follows: Ag as a bottom and top contact, 2,2',7,7'-tetrakis (*N,N'*-di-*p*-methylphenylamino)-9,9'-spirobifluorene (Spiro-TTB) that is p doped with 2,2'-(perfluoronaphthalene-2,6-diylidene)dimalononitrile (F6TCNNQ) (4 wt%) as the HTL; 2,3,9,10,16,17-hexachlorinated boron subphthalocyanine chloride (Cl₆SubPc) and 2,3,6,7-tetrahydro-1,1,7,7-tetramethyl-1H,5H,11H-10-(2-benzothiazolyl) quinolizino-[9,9a,1gh]-coumarin (C545T) as the strong coupling layers; *N,N'*-di(naphthalene-1-yl)-*N,N'*-diphenylbenzidine (NPB) or 1,1-bis[(di-4-tolylamino)-phenyl]cyclohexane (TAPC) as the EBL; NPB or tris(4-carbazoyl-9-ylphenyl)amine (TCTA) as an emitter host layer; bis(2-methylidibeno[f,h] quinoxaline)(acetylacetone)-iridium(III) (Ir(MDQ)₂(acac) at a doping concentration of 10 wt%) or bis[2-(2-pyridinyl-N)phenyl-C](acetylacetone)iridium(III) (Ir(ppy)₂(acac) at a doping concentration of 10 wt%) as the emitting dopants; bis-(2-methyl-8-chinolinolato)-(4-phenyl-phenolato)-aluminium(III) (BAIq) or 4,7-diphenyl-1,10-phenanthroline (BPhen) as the HBL; and BPhen doped with Cs as the ETL. All the organic materials were obtained from Lumtec in sublimed grade and used as received. Layer thicknesses were controlled in situ using calibrated quartz crystal microbalances. Details of the device stack and layer thicknesses for each sample are provided in Supplementary Tables 1–5. Before fabrication, the substrates were cleaned by ultrasonication in acetone, isopropyl alcohol and deionized water (10 min each), followed by O₂ plasma ashing for 3 min. The evaporated devices were encapsulated without exposure to ambient air in a nitrogen atmosphere with a glass lid and moisture getter using ultraviolet-curable epoxy (Norland NOA68). The active area of the devices was 4.0 mm². Flexible devices based on thin-film encapsulation were prepared on cleaned glass carrier substrates, as described elsewhere⁴⁵. In brief, parylene C (diX C, KISCO) and the thin-film oxide layers were deposited using a parylene coater (Labcooter 2, SCS) and an atomic layer deposition reactor (Savannah S200, Ultratech), respectively, with both coaters connected to the evaporator via a common nitrogen-filled glovebox. To accommodate the processing temperature of the atomic layer deposition layers (80 °C), BPhen was replaced by the more stable 2,9-dinaphthalen-2-yl-4,7-diphenyl-1,10-phenanthroline, and a hole injection layer of 1 nm MoO₃ was added between the bottom contact and HTL⁵⁷. Details of the flexible device stack are presented in Supplementary Table 3. After processing, the devices were peeled off the carrier substrate to yield free-standing, flexible OLEDs.

Device characterization

Current density and luminance–voltage behaviour were analysed with a source measure unit (Keithley 2450) and a calibrated amplified Si photodiode (Thorlabs PDA100A) positioned at a fixed distance of 16.7 cm and connected to a digital multimeter (Keithley 2100). Angle-resolved spectra were measured using a goniometer setup built in-house⁵⁸ equipped with a fibre-coupled spectrometer (Ocean Optics Maya LSL). The EQE was calculated by taking into account the angular emission characteristics of the OLED. Angle-resolved reflectivity spectra were recorded using a varying-angle spectroscopic ellipsometer that allowed reflectivity measurements for angles greater than 20° (VASE, M-2000, J.A. Woollam). The optical constants of all the materials were determined using VASE and used to calculate their absorption profiles, electric-field distribution and OLED reflectivity spectra with a transfer

matrix model. The polariton branches were calculated using a CO model⁴³. The photographs of the devices were taken using a digital single-lens reflex camera (Nikon D7100) with a macro lens (Sigma 105 mm F2.8 EX DG OS HSM).

Data availability

The research data supporting this publication can be accessed at <https://doi.org/10.17630/84de9e15-84d4-4445-8131-f372dfbac436>.

References

57. Deng, Y., Keum, C., Hillebrandt, S., Murawski, C. & Gather, M. C. Improving the thermal stability of top-emitting organic light-emitting diodes by modification of the anode interface. *Adv. Opt. Mater.* **9**, 2001642 (2021).
58. Archer, E. et al. Accurate efficiency measurements of organic light-emitting diodes via angle-resolved spectroscopy. *Adv. Opt. Mater.* **9**, 2000838 (2021).

Acknowledgements

We acknowledge funding by the Volkswagen Foundation (no. 93404; M.C.G.), the Leverhulme Trust (RPG-2017-213; M.C.G.), the European Research Council under the European Union Horizon 2020 Framework Programme (FP/2014-2020)/ERC grant agreement no. 640012 (ABLASE; M.C.G) and the Alexander von Humboldt Foundation (Humboldt Professorship; M.C.G.). A.M. acknowledges funding through an individual fellowship of the Deutsche Forschungsgemeinschaft (404587082; A.M.) and from the European Union's Horizon 2020 research and innovation programme under Marie Skłodowska-Curie grant agreement no. 101023743 (PolDev; A.M.).

Author contributions

A.M., S.H. and M.C.G. initiated the study and planned the experiments. A.M., S.K. and S.H. fabricated and measured the electrical performance of the devices. S.H. and S.K. optimized the reference OLEDs. A.M. and S.K. fabricated and analysed the flexible devices. A.M. performed the angle-resolved reflectivity and ellipsometry measurements, device photography and calculations using the CO and transfer matrix models. All the authors analysed and discussed the data. A.M. and M.C.G. wrote the paper with contributions from all the authors.

Funding

Open access funding provided by Universität zu Köln.

Competing interests

The authors declare no competing interests.

Additional information

Supplementary information The online version contains supplementary material available at <https://doi.org/10.1038/s41566-023-01164-6>.

Correspondence and requests for materials should be addressed to Andreas Mischor or Malte C. Gather.

Peer review information *Nature Photonics* thanks the anonymous reviewers for their contribution to the peer review of this work.

Reprints and permissions information is available at www.nature.com/reprints.